The Evolving Internal Structure of Ineffective Filters during Erosion

Adnan Sufian[1*], Tilman Bittner[2], Thierry Bore[1], Mathieu Bajodek[3] and Alexander Scheuermann[1]

[1]School of Civil Engineering, The University of Queensland, Australia
[2]Eisenbahn-Bundesamt (Federal Railway Authority), Hamburg, Germany
[3]Laboratoire d'analyse et d'architecture des systèmes (LAAS–CNRS), Université de Toulouse, Toulouse, France.
[*] Corresponding author (email: a.sufian@uq.edu.au)

ABSTRACT

Filters play an important role in mitigating internal erosion failure in dams. When filters are ineffective, the transport of finer base particles into the filter results in a change in the internal structure, with a reduction in the porosity as base particles fill the pore space formed by filter particles. This paper presents the results of filtration experiments conducted using a copper-built permeameter, which acted as a coaxial transmission line enabling the spatial and temporal evolution of local porosity to be determined using spatial time domain reflectometry. A porosity field map was constructed providing a graphical representation of the evolving internal structure, from which the onset and rate of progression could be quantified. The key outcome was the quantitative characterization of the filtration process by both the transport of base particles into the filter and the settlement of the filter particles into the base layer.

INTRODUCTION

Internal erosion is a major cause of failure for water retaining structures such as dams and levees. Internal erosion occurs when soils particles within the body of a dam or its foundations are dislodged and migrated with seepage flows. Foster et al. (2000) indicated that 46% of dam failures were attributed to internal erosion, highlighting the importance of better understanding the internal erosion process and developing new approaches to quantitively explore the internal structure.

Filters play a central role in mitigating internal erosion failure. A filter is generally composed of a coarser granular soil, and is placed adjacent to a finer soil, termed the base soil. Filters have two key functions; a retention function to prevent the wash out of the finer base soil, and a drainage function to ensure that excess pore water pressure does not build up behind the filter. Modern filter design aims to specify a range of particle size distributions for the filter soil to meet these two functions. However, existing filters may not meet the requirements of modern filter design, and for existing ineffective filters, it remains a challenge to understand how the internal erosion process evolves from the onset condition to progression to washout of finer base particles.

Foster & Fell (2001) proposed geometric criteria based on the particle size distributions of the filter and base soils to delineate the 'no erosion', 'excessive erosion' and 'continuing erosion' boundaries for existing filters. This study will focus on those filters that meet the 'continuing erosion' criteria proposed by Foster & Fell (2001) and are termed ineffective filters in this paper. Ineffective filters lead to the migration of base particles into the filter, resulting in a change in the internal structure of the filter. The focus on ineffective filters enables the complete internal erosion process to be explored.

Existing approaches to measure the evolving internal structure of filters are typically based on macroscopic observations and point measurements in laboratory experiments. Ineffective filters result in the mixing of base and filter particles which leads to a change in the porosity distribution along the sample. Different methods have been considered to determine the porosity distribution in physical laboratory experiments, including observation of changes in layer heights (Ke & Takahashi, 2012) and washed out particles (Rochim et al., 2017), use of gamma rays (Sibille et al., 2015), computed tomography scans (Homberg et al., 2012) and electromagnetic methods using spatial time domain reflectometry (spatial TDR) (Scheuermann et al. 2010).

This paper demonstrates how physical observations obtained using spatial TDR can provide new insights into the evolving internal structure of ineffective filters. Relative to other above-mentioned approaches, spatial TDR can determine the evolving local porosity along the permeameter with good accuracy and reasonable temporal and spatial resolution. A purpose-built coaxial cell permeameter (Bittner et al., 2019) is utilised to conduct filtration experiments at different size ratio of base and filter particles, and a graphical representation of the evolving internal structure is presented to quantify the onset and progression during the filtration process.

EXPERIMENTAL METHODOLOGY

The coaxial cell permeameter consisted of a coaxial erosion cell, a closed water cycle system, and various instrumentation, as schematically illustrated in Figure 1. A detailed description of the experimental apparatus is presented in Bittner et al. (2019), and only a summary of key elements of the apparatus is presented below. The copper-built erosion cell acts as a coaxial transmission line enabling electromagnetic measurements of the porosity distribution along the sample. A 45 cm long sample can be prepared within the annulus formed by the inner and outer conductors of the cell. An inner and outer conductor was required to ensure that the electric field was perfectly boundary between the conductors. The inner conductor has an outer diameter of 41.3 mm and the outer conductor has an inner diameter of 151.9 mm. A 4 cm wide and 42 cm high observation window on the outer surface of the cell enabled visual observation of the filtration process. Electromagnetic measurements were obtained using a time domain reflectometer. The porosity distribution along the cell could be determined from the TDR trace using an inversion technique, which is detailed in Sufian et al. (2022). Upwards flow was considered in the coaxial erosion cell

with seepage from an upstream constant head overflow tank which could be adjusted to apply different hydraulic head. A constant overflow was maintained at the top of the cell ensuring a constant total head downstream of the sample. All connecting pipes had an inner diameter of 32 mm to minimise the head loss through the pipes and a flow homogeniser was placed at the base of the cell to achieve a relatively uniform flow condition. The flow rate was measured using a flowmeter, and 14 pressure transducers enabled the measurement of pore water pressure.

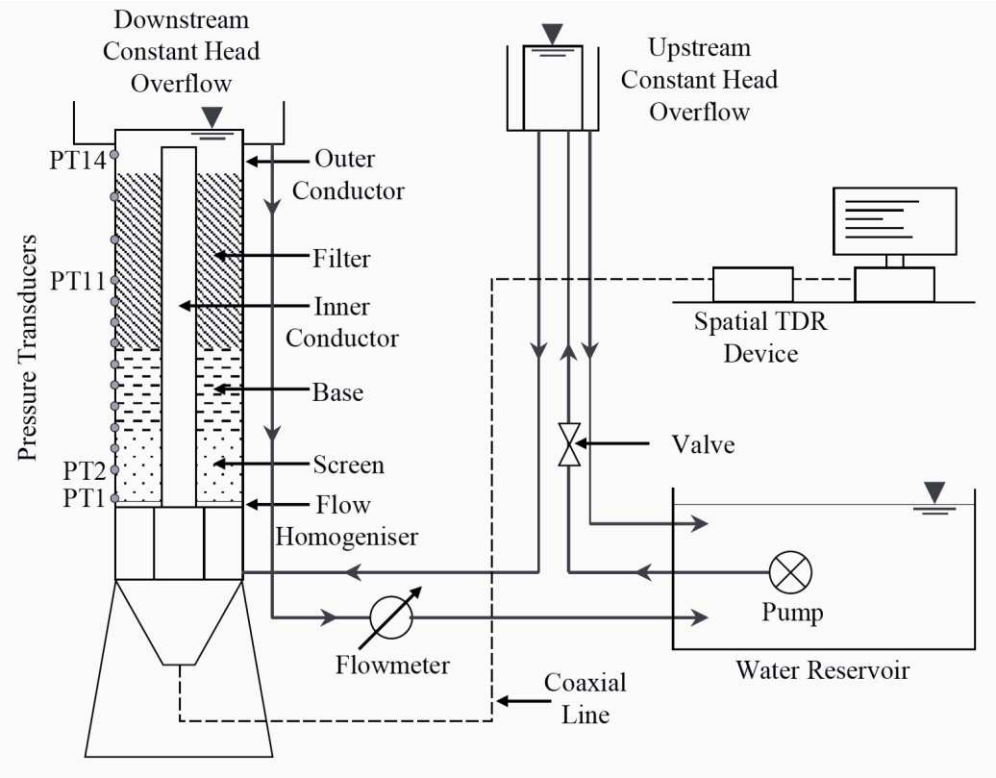

Figure 1: Sample setup for filtration experiments using the coaxial cell permeameter

Base-filter samples for filtration experiments were prepared with soda-lime glass beads as an idealised granular soil. Glass beads are advantageous from a spatial TDR perspective due to the constant dielectric permittivity of the glass beads, which simplifies the inversion procedure. The sample consisted of a screening layer, overlaid by the base layer, which is overlaid by the filter layer (Figure 1). The screening layer ensured that base particles did not experience significant downwards penetration into the screening layer and consisted of an approximately 5 cm layer of 6 mm diameter glass beads, underlying an approximately 4 cm layer of 2 mm diameter glass beads. Two different diameter glass beads were considered for the base and filter layers:

- Base I: particle sizes ranging from 0.425 - 0.600 mm
- Base II: particle sizes ranging from 0.300 - 0.425 mm
- Filter A: particle sizes of 8 mm
- Filter B: particle sizes of 6 mm

The base layer was approximately 10 cm in height, while the filter layer was approximately 20 cm in height. The filter particles are approximately monodisperse, while the base particles exhibited a narrow size range due to the manufacturing process. Four different base-filter combinations were formed with the two base and filter soils: (i) BI_FA (Base I and Filter A); (ii) BI_FB; (iii) BII_FA; and (iv) BII_FB. All base-filter combinations satisfied the Foster & Fell (2001) 'continuing erosion' criteria which is defined by the ratio $d_{15F}/d_{95B} > 9$. The d_{15F}/d_{95B} size ratio ranged from 10.2 for BI_FB to 19.2 for BII_FA, and hence, all samples can be regarded as ineffective filters. The porosity of the base layer was similar in all four samples, ranging from 0.36 to 0.38, and the porosity of the filter layer was also similar (ranging from 0.37 to 0.39). Filtration experiments were conducted with upward flow with the applied hydraulic head increasing 1 cm every 10 minutes. The test was concluded when there was breakthrough of the base particles through the filter layer and fluidisation of the base particles was visually observed at the top of the coaxial erosion cell.

EVOLUTION OF INTERNAL STRUCTURE

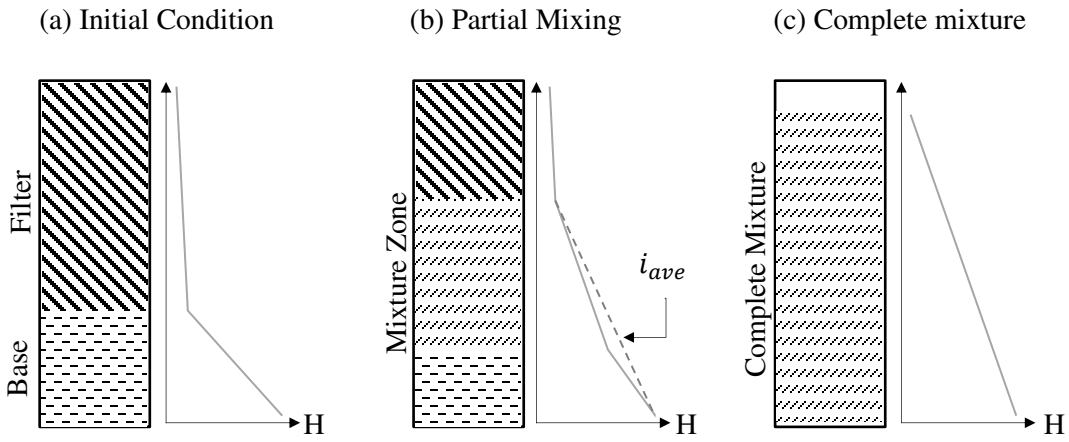

Figure 2: Schematic illustration of a typical filtration experiment

The key stages of the filtration experiment are schematically shown in Figure 2 along with the distribution of the total head along the sample. Initially, the base and filter materials are distinct layers (Figure 2a). Head loss is dominated in the base layer and the hydraulic gradient in the base layer can be calculated from the pressure transducers within the base layer. With the onset of erosion, a mixture zone consisting of base and filter particles is formed (Figure 2b). While this is conventionally assumed to be the result of the transport of base particles into the filter under upward seepage flow, the subsequent analysis of the spatial TDR data will demonstrate that the settling of the filter particles into the base layer also has a significant contribution to the formation of the mixture zone. Head loss occurs in both the base layer and the mixture zone, while minimal head loss is noted in the filter layer as the hydraulic conductivity of the filter layer is significantly higher than the base layer and the mixture zone. The hydraulic gradient can be determined from the pressure transducers in the base layer and mixture zone. However, due to the spacing between

pressure transducers, it was not possible to assess the hydraulic gradient in the mixture zone in the early stages of the mixing process, and in the base layer prior to complete mixing. Hence, an average gradient is considered across the base layer and mixture zone, as shown in Figure 2b. The conclusion of the experiment was marked by the formation of a complete mixture of the base and filter layer (Figure 2c) and generally some settlement is also noted as the mixture of base and filter particles form a denser packing than the distinct base and filter layers in the initial condition. Head loss occurs across the entire length of the sample, and the average hydraulic gradient is obtained from the pressure transducers within the complete mixture.

While the hydraulic gradient is typically obtained in conventional permeameter experiments, the use of spatial TDR in this study enabled the determination of the local porosity profile along the sample length via an inversion procedure. A typical porosity profile is shown in Figure 3 for the partial mixing condition schematically illustrated in Figure 2b. The local porosity profile is compared with the average porosity profile obtained from the conventional approach considering the dry mass added and the layer thickness. Note that unlike the local porosity profile obtained from spatial TDR, the average porosity profile is constant across the layer. A good agreement is noted between both approaches. While the conventional approach is simple and intuitive, it has a major limitation in that evolving internal structure cannot be readily tracked. In contrast, the near continuous spatial TDR measurements enable the evolution of the porosity profile to be quantified by stitching together discrete local porosity profiles to form a porosity field map.

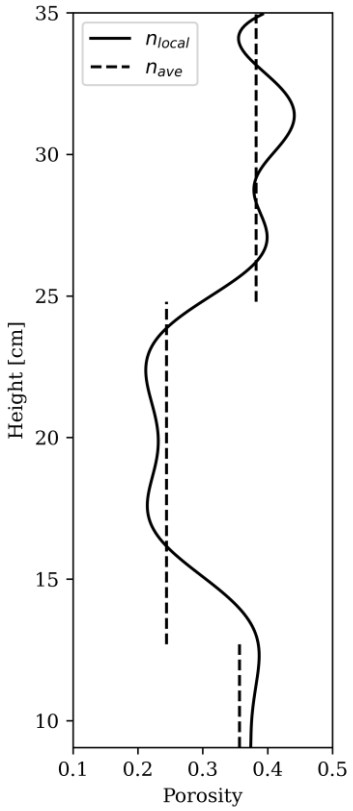

Figure 3: Comparison of local and average porosity

A typical porosity field map is shown in Figure 4. The porosity field map provides a graphical representation of the local porosity obtained from spatial TDR along the sample height and for the duration of the experiment. The three conditions schematically illustrated in Figure 2 can be readily observed in the porosity field. Initially, the base and filter layer are distinct, but because the porosity of the base and filter layer are similar, minimal differences are noted in the porosity field map. Annapareddy et al. (2023) presented an alternate field map based on the local permeability, which is capable of distinguishing between the base and filter layer in the initial condition. Following the onset of filtration, the formation of the mixture zone is clearly visible in the porosity field map by the darker shaded region (indicative of a reduction in the porosity). The complete mixture is signified by a darker shaded region across the sample height, along with some settlement of the sample which is visualised by the lighter shaded region (due to the increase in the porosity). These visual observations of the porosity field map can be quantified by three characteristic lines:

1. Lower limit of the mixture zone, $h_{lower}(t)$
2. Upper limit of the mixture zone, $h_{upper}(t)$
3. Settlement line, $h_{settle}(t)$

which are illustrated in Figure 4. The onset condition can be inferred from the intersection of $h_{lower}(t)$ and $h_{upper}(t)$, while the rate of progression can be inferred from the gradient of $h_{lower}(t)$ and $h_{upper}(t)$. The gradient of $h_{settle}(t)$ is indicative of the rate of settlement and can also be used to obtain the final height of the sample. The three characteristic lines are determined by considering the absolute gradient of the porosity field along the sample height, which is subsequently filtered by setting those points with an absolute gradient less than some threshold value to zero, after which a line of best-fit was considered to define the characteristic lines. The best-fit characteristic lines are shown in Figure 4 and agree well with visual observations of the layer heights in the observation window. Therefore, a quantitative assessment of the entire filtration process from onset to progression to complete mixture can be obtained from the porosity field map.

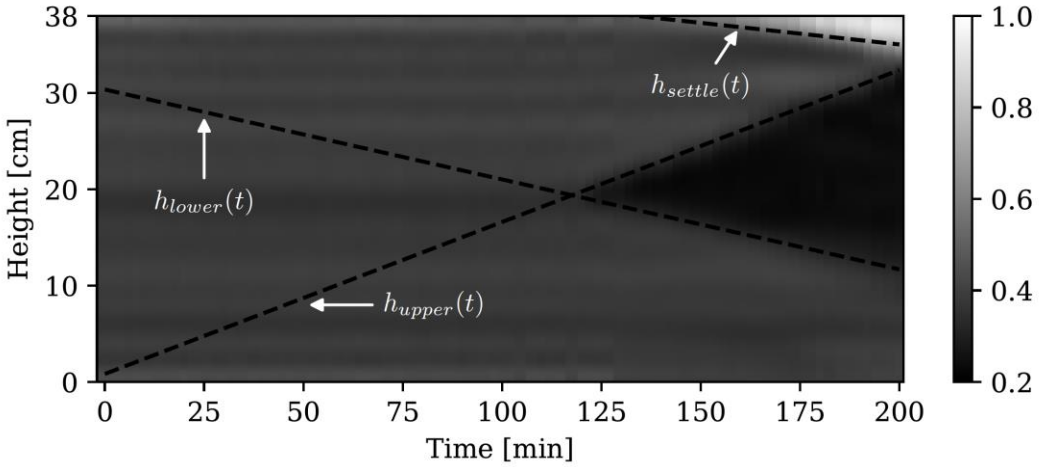

Figure 4: Typical example of a porosity field map (Sample BI_FA)

In physical experiments, it is challenging to observe the limiting onset condition because base particles are on the cusp of migrating into the filter layer. However, it can be readily inferred from the porosity field map by the intersection of the lower and upper limits of the mixture zone. The limiting onset condition is shown by the intersection of dashed lines for $h_{upper}(t)$ and $h_{lower}(t)$ in Figure 4. In addition, the hydraulic gradient at the limiting onset condition, i_{onset}, can be obtained from the pressure transducers and is listed in Table 1. i_{onset} showed a strong dependence on the size of the filter particles with a lower i_{onset} noted for larger filter particles. This is expected because larger filter particles provide larger constrictions for base particles to migrate more freely. When the constrictions are significantly large, i_{onset} is expected to approach the Terzaghi critical hydraulic gradient (i_{crit}), which is also listed in Table 1. For samples with Filter A (larger filter particles), Table 1 indicates that $i_{onset} \approx i_{crit}$, while $i_{onset} > i_{crit}$ for samples with Filter B.

Table 1: Key Onset and Progression Characteristics

Sample	i_{onset}	i_{crit}	m_{upper} (cm/min)	m_{lower} (cm/min)	m_{settle} (cm/min)	h_{final} (cm)
BI_FA	0.96	0.93	0.16	-0.09	-0.04	35.0
BI_FB	1.17	0.95	0.21	-0.09	-0.03	35.2
BII_FA	0.93	0.96	0.08	-0.03	-0.02	36.2
BII_FB	1.18	0.96	0.11	-0.04	-0.02	36.5

The progression of filtration is quantitatively characterised by the gradient of the lower limit of the mixture zone, m_{lower}, and the gradient of the upper limit of the mixture zone, m_{upper}, which are listed in Table 1. A key observation is that $|m_{upper}| > |m_{lower}|$ for all base-filter combinations with $1.5 < |m_{upper}/m_{lower}| < 3.0$. This is indicative of the two concurrent processes during the progression of filtration: (i) transport of base particles into the filter layer by seepage flow; and (ii) settlement of the filter particles into the base layer. The settlement of the filter particles is a result of local partial bearing failure surrounding the contact point of the filter particle with the effective stress reducing at the base-filter interface with increasing applied head for upward flow. m_{lower} captures the rate of settlement of filter particles into the base layer, while m_{upper} captures the process of base particle migration due to seepage flow as well as displacement of base particles due to settlement of filter particles. m_{lower} and m_{upper} is primarily dependent on the size of the base particles, with the rate increasing with increasing base particle size. Hence, a higher rate of growth of the mixture zone was noted for experiments with Base I. This is believed to be a result of increased frequency of collisions between the smaller base particles, which leads to greater energy dissipation for the base particles, and consequently, the formation of a smaller mixture zone.

The settlement of the sample with the progression of filtration is captured by the settlement line. The gradient of the settlement line, m_{settle}, reflects the rate of settlement and is listed in Table 1. Similarly to the gradient of the upper and lower limits of the mixture zone, m_{settle} is also larger

for the larger base particles in Base I, and consequently, the final height of the sample is smaller for tests with Base I. Note that the complete mixture formed very quickly, and hence, the gradients of the upper and lower limits of the mixture zone may not coincide with the final height of the sample based on the settlement line.

CONCLUSION

This paper presents the outcomes of a set of filtration experiments conducted using the coaxial cell permeameter, which enabled the determination of the local porosity profile along the sample using spatial time domain reflectometry. By considering ineffective base-filter combinations that produced continuing erosion, the entire internal erosion process from onset to progression to complete mixture of the base and filter layer could be investigated. A graphical representation of the evolving internal structure was presented in the form of a porosity field map, from which quantitative characteristics of the onset and progression could be determined. It was observed that the onset was influenced by the size of filter particles, while the progression was influenced by base particle size. A key outcome was that the formation of the mixture zone was a result of two processes; the migration of base particles into the filter layer, and the settlement of the filter particles into the base layer. The growth of the mixture zone was postulated to be an outcome of the inter-particle collisional energy dissipation of base particles. However, these processes cannot be readily observed in the coaxial cell permeameter and further research with the aid of fluid-particle numerical simulations are required to explore this phenomenon.

REFERENCES

Annapareddy, V.S.R., Sufian, A., Bore, T., Bajodek, M. and Scheuermann, A., 2022. Computation of local permeability in gap-graded granular soils. Géotechnique Letters, 12(1), pp.68-73.

Bittner, T., Bajodek, M., Bore, T., Vourc'h, E., and Scheuermann, A. 2019. Determination of the porosity distribution during an erosion test using a coaxial line cell. Sensors, 19(3): 611.

Foster, M., and Fell, R. 2001. Assessing embankment dam filters that do not satisfy design criteria. Journal of Geotechnical and Geoenvironmental Engineering, 127(5): 398–407.

Foster, M., Fell, R., and Spannagle, M. 2000. The statistics of embankment dam failures and accidents. Canadian Geotechnical Journal, 37(5): 1000– 1024.

Homberg, U., Baum, D., Prohaska, S., Kalbe, U., and Witt, K. 2012. Automatic extraction and analysis of realistic pore structures from lCT data for pore space characterization of graded soil. Zuse Institute, Berlin.

Ke, L., and Takahashi, A. 2012. Strength reduction of cohesionless soil due to internal erosion induced by one-dimensional upward seepage flow. Soils and Foundations, 52(4): 698–711.

Rochim, A., Marot, D., Sibille, L., and Thao Le, V. 2017. Effects of hydraulic loading history on suffusion susceptibility of cohesionless soils. Journal of Geotechnical and Geoenvironmental Engineering, 143(7): 04017025.

Scheuermann, A., Heubner, C., Wienbroer, H., Rebstock, D., and Huber, G. 2010. Fast time domain reflectometry (TDR) measurement approach for investigating the liquefaction of soils. Measurement Science and Technology, 21(2): 025104.

Sibille, L., Marot, D., and Sail, Y. 2015. A description of internal erosion by suffusion and induced settlements on cohesionless granular matter. Acta Geotechnica, 10(6): 735–748.

Sufian, A., Bittner, T., Bore, T., Bajodek, M. and Scheuermann, A., 2022. Physical observations of the transient evolution of the porosity distribution during internal erosion using spatial time domain reflectometry. Canadian Geotechnical Journal, 59(8), pp.1443-1458.